Geomechanics and Engineering, *Vol. 34, No. 2 (2023) 139-154*
https://doi.org/10.12989/gae.2023.34.2.139

Geophysical and mechanical investigation of different environmental effects on a red-bed soft rock dam foundation

Liming Zhou, Yujie Li*, Fagang Wang and Yang Liu

Key Laboratory of Geotechnical Mechanics and Engineering of Ministry of Water Resources, Changjiang River Scientific Research Institute, Wuhan, Hubei 430010, China

(*Received December 28, 2022, Revised April 7, 2023, Accepted April 18, 2023*)

Abstract. Red-bed soft rock is a common stratum and it is necessary to evaluate the mechanical properties and bearing capacity of red-bed soft rock mass affected by different environmental effects. This paper presents a complete procedure for evaluating the bearing capacity of red-bed soft rock by means of geophysical exploration and *in-situ* rock mechanics tests. Firstly, the thickness of surface loosened rock mass of red-bed soft rock was determined using geophysical prospecting method. Then, three environmental effects, including natural weathering effect, dry-wet cycling effect and concrete sealing effect, were considered. After each effect lasted for three months, in-situ rock mass mechanical tests were conducted. The test results show that the mechanical properties of rock mass considering the sealing effect of concrete were maintained. After considering the natural weathering effect, the mechanical parameters decrease to a certain extent. After considering the effect of dry-wet cycling, the decreases of mechanical parameters are the most significant. The test results confirm that the red-bed soft rock dam foundation rock mass will be significantly affected by various environmental effects. Therefore, combined with the mechanical test results, some useful implementations are proposed for the construction of a red-bed soft rock dam foundation.

Keywords: dam foundation; dry-wet cycling; geophysical prospecting; *in-situ* mechanical testing; natural weathering; red-bed soft rock

1. Introduction

The red-bed mainly refers to diagenetic clastic rocks of the Triassic, Jurassic, Cretaceous, and Cenozoic Paleogene since Mesozoic, which are classified as belonging to lacustrine facies, fluvial facies, fluvial-lacustrine facies or piedmont proluvial facies: as the appearance of the stratum is mainly red, it is called a red-bed. Red-beds are mostly interbedded, and three indices are commonly used for the discrimination of red-bed, namely, the color being reddish to the naked eye, the environment of continental sedimentation, and the conditions of clastic sedimentation prevailing. The red-bed strata lithology is mostly mudstone, shale, silty mudstone, and other argillaceous soft rocks. Affected by lithological conditions, the red bed soft rock has typical characteristics of low permeability, strong hydrophilicity, ready softening (or expansion) when exposed to water, easy disintegration (or shrinkage) under dehydration, and poor mechanical properties. Currently, many scholars have conducted research into red-bed soft rocks. On formation mechanisms thereof, Trümper *et al*. (2020) studied fluvial red beds containing preserved large woody debris and provided evidence for the concurrence of river depositional systems and vegetation. Huang *et al*. (2020) performed Mossbauer spectroscopic and petrographic studies on red beds in the eastern Tibetan Plateau to discuss the mechanism of remagnetization. Aehnelt *et al*. (2021) studied the red bed sediments of Triassic Buntsandstein deposits and explored the origin of bleaching phenomena. In structural geological terms, Wilmsen *et al.* (2021) investigated the upper Jurassic Garedu red bed formation in the northern Tabas Block and elucidated the tectonics thereof. Marat *et al.* (2022) conducted a comprehensive investigation of red bed slopes in Romania and found that the interactions between stratum and water infiltration form the driving mechanism for landslide reactivation. Yan *et al.* (2019) combined the distribution of red beds and over 1000 Danxia landform sites to summarize the spatial patterns and geological elements. In terms of their mechanical properties, Azarafza *et al.* (2019) studied the geotechnical characteristics of dark red beds in Iran and proposed empirical relationships between them. Koshnaw *et al.* (2019) investigated red-bed series strata in Iraq and discussed evidence indicating the time of Arabia-Eurasia continental collision. Zhou *et al.* (2021) focused on the red-bed soft rock from the Three Gorges Reservoir area in China and studied the water-rock interaction at mesostructured level. Liu *et al.* (2019) examined the behavior of red-bed soft rock under seawater condition and studied its softening mechanism and control measures. Zhou *et al*. (2019) attempted to classify red-bed rock mass structures and summarized slope failure modes in south China. Shen *et al*. (2018) studied the slaking properties of red-bed mudstones collected from the Three Gorges Reservoir area.

Red-beds in China are mainly distributed in the south-west and north-west regions. Meanwhile, as the key area of

*Corresponding author, Associated Professor
E-mail: magicbunny@163.com

ISSN: 2005-307X (Print), 2092-6219 (Online)

hydropower resource development, many hydropower stations are under construction or are to be built in south-western China, making the use of red-bed soft rock as a dam foundation inevitable under certain circumstances. Therefore, it is necessary to perform an accurate evaluation of the rock mass mechanical properties and a reasonable assessment of the bearing capacity of dam foundations. Regarding this issue, Shahrbanouzadeh *et al.* (2015) studied seepage conditions pertaining to a dam foundation using FEM and ANN models for Shahid Abbaspour dam. Varmazyari *et al.* (2021) took the dam and reservoir as a single entity to study the influences of different earthquake-input mechanisms on the foundation. Wu *et al.* (2019) proposed an approach to identify the geomechanical parameters required for deformation modulus of arch dams. Yilmaz *et al.* (2021) compared the deformation modulus of a dam foundation rock mass derived from *in-situ* measurement and plate loading tests. Moreover, scholars performed further research on other relevant and important aspects, such as the failure analysis of a dam foundation (Jiang 2019, Wang 2020) and reinforcement techniques (Chen 2012, Jiang 2021). Chen *et al*. (2023) proposed an energy-frequency parameter to evaluate the intensity measure for earthquake ground motion.

Many researchers have investigated the mechanical properties and modelling techniques of red-bed soft rock. He *et al*. (2023) investigated the mechanical properties of red-bed soft rock subjected to freeze-thaw cycles and proposed a modified binary-medium constitutive model. Liu *et al*. (2019) studied the influence mechanism of different flow patterns on the softening of red-bed soft rock. Li *et al.* (2023) focused on the shear-creep behavior of weak interlayer mudstone in a red-bed soft rock in acidic environments and proposed an improved Burgers model. Yu *et al.* (2022) studied the critical damage point of the red-bed soft rock during damage and destruction using multiple approaches. Zhang *et al.* (2020) compared the effects of different test methods on the disintegration of red-bed soft rock and proposed a model predicting the evolution of disintegration under cyclic wetting and drying. Although abundant achievements have been made through the aforementioned research into the characteristics of red-bed soft rock, work on the mechanical characteristics of red-bed soft rock as dam foundation rock mass, especially the variations in mechanical properties of the red-bed dam foundation under factors such as naturally weathering, dry-wet cycling, and dam concrete sealing remains sparse. The rock mass of the dam foundation will undergo excavation, concrete backfilling, and weathering during construction. Besides, the potential wetting effect of rainfall and its subsequent evaporation will cause the rock mass to experience cyclic wetting-drying during the reinforcement of a dam foundation. Therefore, it is necessary to evaluate the variations in mechanical properties under different practical effects for red-bed soft rock, which is easily disturbed by excavation and may soften or even disintegrate when exposed to water. This paper proposes a comprehensive investigation of the mechanical properties of red-bed soft rock under weathering and dry-wet cycling effects. The geophysical prospecting technique and *in-situ* mechanical testing method are both employed to clarify the behavior of a rock mass, which is intended for use in a dam foundation, under different working scenarios. It is highlighted that the geophysical prospecting method is useful to determine the loosened thickness of surface rock mass, to provide practical guidance to actual engineering design. Moreover, the test results reveal that the red-bed soft rock mass will be affected by various environmental effects to varying degrees, so measures should be taken to avoid the influences of environmental factors that cause significant changes in mechanical properties.

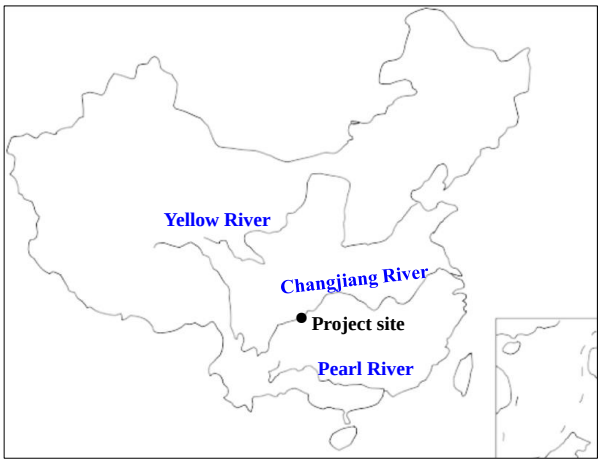

Fig. 1 Location of the project

2. Procedures and methods

2.1 Project outline

The project taken in the present research as a case study is a scheduled hydropower station on Changjiang River in south-west China (Fig. 1). According to the current geological survey and site selection, the dam foundation rock mass in the hydropower project area is mainly composed of red clayey siltstone and silty claystone of Suining Formation of the Upper Jurassic System, which is a typical red-bed soft rock (Fig. 2).

Based on a geological survey, the red-bed rocks of project site can be rapidly weathered after exposure to air, disintegrated after dehydration, and weakened and swelled after immersion in water. Moreover, the high content of montmorillonite in the rock mass of the dam foundation makes the dam foundation prone to uplift deformation, which is not conducive to the structural safety of dam structure. It is based on above findings that the emphasis of the present study is placed on the extent of weathering extent of red-bed soft rock mass and the characterization of its mechanical properties under different working scenarios.

2.2 Procedure

The combination of *in-situ* testing with laboratory tests was used to explore the mechanical properties of rock mass of the red-bed soft rock dam foundation under various

Fig. 2 Image of the red-bed at the project site

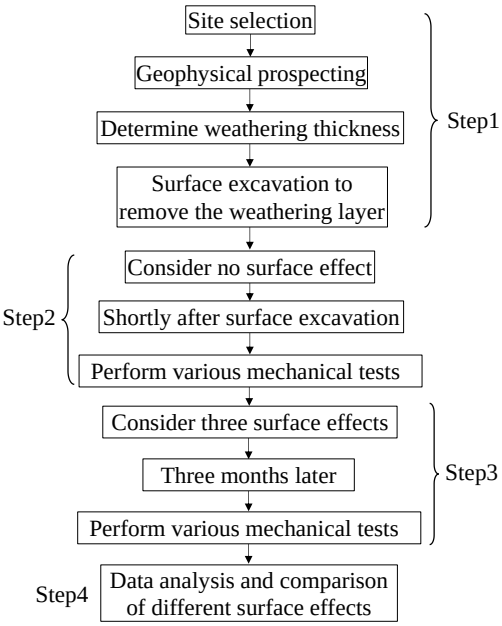

Fig. 3 Flowchart through the investigation

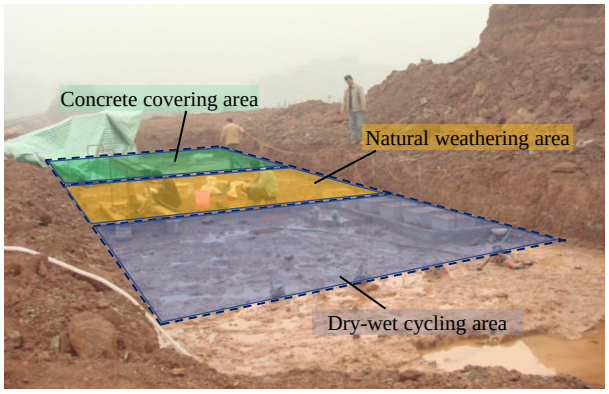

(a) Site image

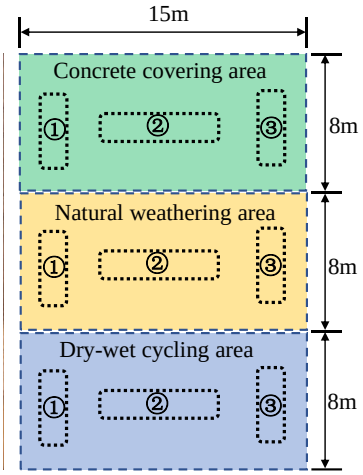

(b) Plan view

Fig. 4 Site image and zones of the testing area: ① Site for rock mass deformation testing; ② Site for geophysical prospecting; ③ Site for direct shear testing of the rock-concrete interface

environments. Considering that the rock mass of the actual dam foundation has not yet been excavated, an area with the same lithology and similar rock mass structure characteristics to those at the actual dam site could be selected. Considering that the shallow and surface layer of the red-bed soft rock in the test area is natural terrain and has been affected by long-term weathering, it cannot meet the requirement that the rock mass of the dam foundation should be in slightly weathered or non-weathered strata, the method that combines geophysical prospecting and mechanical test was adopted to conduct the investigation. The flowchart through the procedure is shown in Fig. 3.

The whole process can be divided into five steps.

Step 1. The testing site that has similar geological characteristics to the rock masses at the dam foundation is selected. The surface loosened natural rock masses are then removed based on estimation by geophysical prospecting.

Step 2. The site is divided into four areas and a series of rock mechanical tests are performed shortly after the surface excavation in any one of the divided areas. These tests include *in-situ* rock mass deformation tests, *in-situ* direct shear test of rock-concrete interface, and medium-sized rock sample shear tests performed in a laboratory. The stiffness and strength parameters of rock mass can thus be obtained as a baseline for evaluating the mechanical property of red-bed soft rock under various environmental conditions.

Step 3. For the remaining three areas (Fig. 4), three surface effects are considered for each area: 1) natural weathering, whereby the rock mass is directly exposed to air without any artificial treatment and subjected to natural weathering for three months; 2) dry-wet cycling, whereby the surface is first filled with water to remain soaked for seven days and then drained to expose it to air for another seven days, which process is then repeated for three months; 3) concrete covering, whereby the surface is covered with concrete to eliminate the influences of water and air on the covered rock mass. The three surface effects correspond to the various environmental conditions to which a dam foundation may be subjected during construction. Thus, the variations in mechanical properties of the red-bed soft rock dam foundation may be quantified.

Step 4. Data analysis and comparison of the resulting

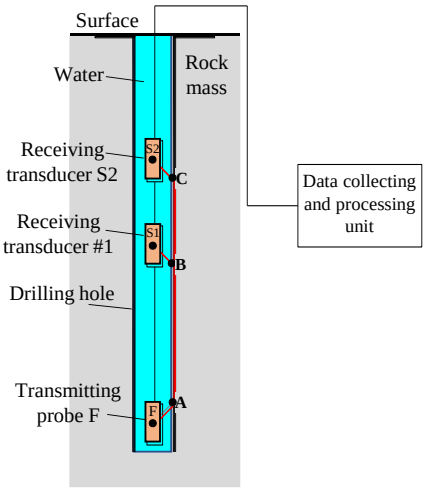

Fig. 5 Borehole acoustic testing technique

mechanical parameters are performed to investigate the influences of different surface effects on a red-bed soft rock dam foundation.

2.3 Geophysical prospecting methods for detecting weathering in the rock mass

2.3.1 Geophysical prospecting using single-hole acoustic wave velocity index

By using the different propagation and absorption characteristics of different geotechnical bodies, the sound waves propagating from the source can be received by instantaneous or repeated impact on the geotechnical media under test, thus obtaining the sound wave velocity. Then, the engineering properties of the geotechnical media can be obtained according to the variation of wave velocity. The borehole acoustic testing technique is further illustrated in Fig. 5 and is explained below.

Assuming the longitudinal velocity of the fluid in the borehole is V_1 and the longitudinal velocity of the rock layer at the borehole wall is V_P, the path of the sound wave to the receiving probe S_1 is $F \rightarrow A \rightarrow B \rightarrow S_1$ and the time taken is

$$t_1 = \frac{\mathrm{FA}}{V_1} + \frac{\mathrm{AB}}{V_P} + \frac{\mathrm{BS1}}{V_1} = \frac{2\mathrm{FA}}{V_1} + \frac{\mathrm{AB}}{V_P} \tag{1}$$

Similarly, the time taken for propagation of the sound wave from F to S_2 is

$$t_2 = \frac{\mathrm{FA}}{V_1} + \frac{\mathrm{AC}}{V_P} + \frac{\mathrm{CS2}}{V_1} = \frac{2\mathrm{FA}}{V_1} + \frac{\mathrm{AC}}{V_P} \tag{2}$$

The propagation time difference is

$$\Delta t = t_2 - t_1 = \frac{BC}{V_p} = \frac{L_d}{V_P} \tag{3}$$

This gives the average wave velocity at the BC section of the pore wall

$$V_P = \frac{L_d}{t_2 - t_1} \tag{4}$$

According to the above principle, the wave velocity of rock mass in each measuring section is calculated, and the curve of wave velocity variation with hole depth is drawn.

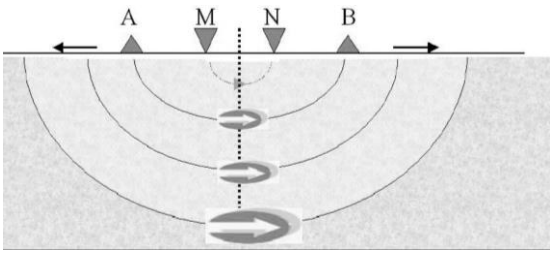

Fig. 6 The electrical prospecting method

Based on the hole depth curve of wave velocity, the variation characteristics of longitudinal rock mass properties can be determined, that is, the weakening (and its extent) of the surface soft rock can be determined.

2.3.2 Geophysical sounding methods based on resistivity indicators

The electrical prospecting method was used to detect underground geological structure and underground electrical inhomogeneous body by observing the electrical differences of spatial or temporal distribution characteristics and variations between rocks and ores. The rock mass electrical resistivity ρ was calculated by measuring the current intensity I_{AB} of the power supply circuit and the potential difference $\triangle V_{MN}$ between the measuring electrodes M and N (Fig. 6).

$$\rho = k \frac{\Delta V_{MN}}{I_{AB}} \tag{5}$$

where $k = 2\pi\alpha$.

The principle of the Wenner device is such that: when measuring, the supply electrodes A and B and the measuring electrodes M and N are disposed symmetrically with the measuring point and the distance between them is fixed. The electrode pitches AM, MN and NB are equal. A, M, N and B are moved simultaneously to the right point-by-point, and the potential difference and current strength are observed point-by-point along the profile to calculate the apparent electrical resistivity. As the electrode spacing increases, the apparent electrical resistivity observed point-by-point reflects the distribution of the electrical properties of the layer of the observed rock mass with increasing depth.

2.4 Methods for determining the mechanical properties

2.4.1 Deformation testing

In the selected test area, the location of the test was determined according to the on-site geological conditions. Then, the surface loosened rock mass was removed manually to level an area of 2 m^2. Further, a plane with a diameter of 700 mm was chiselled by hand, and then ground into a horizontal round surface with a diameter of 600 mm with a grinding wheel. After being washed and dried, a geological description was recorded. We aligned and levelled the rock surface with pure cement slurry dosed with a small amount of early strength admixture to ensure intimate contact with the bearing plate, and wait for it to

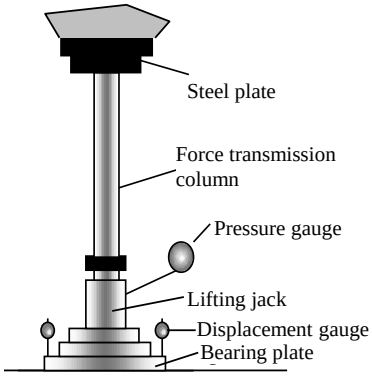

Fig. 7 Installation of the rock mass deformation test

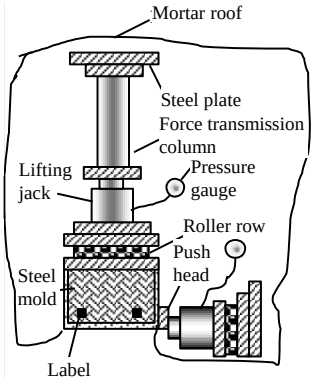

Fig. 8 Field installation of the direct shear test device

cure. On the second day, the force transmission system of the bearing plate and the measuring system required for the test were installed. On the third day, the rock mass deformation test could be conducted. The *in-situ* installation of the device is shown in Fig. 7.

A circular rigid bearing plate with an area of 200,000 mm^2 was adopted. The deformation of the underlying rock mass was measured by dial gauge (1/‰ mm), and the test pressure was measured by standard pressure gauge with a precision of 0.4. The maximum test pressure was 2 MPa, and the pressure was applied in five stages. The pressure was increased by an increase-release circulation in a step-wise manner, and the pressure recorded immediately after the pressure had been increased and released, and then read once every 10 minutes thereafter. When the deformation readings were relatively stable, the next load increment can either be applied or withdrawn.

2.4.2 Direct shear test of the concrete-rock interface

The test was conducted using a horizontal pushing method, with a shear surface area of 500 mm × 500 mm and a maximum positive stress of 2 MPa applied. A horizontal surface measuring 700 mm × 800 mm was chiselled by hand at the selected location, with the undulation difference controlled to within 5 mm to 10 mm.

The concrete strength shall meet the requirements of C20 grade. Ordinary Portland cement of Grade 32.5 shall be selected. The sand and stone were taken from the local quarry, and 1% calcium chloride was added as the early strength agent. A layer of cement mortar with a thickness of 20 mm was placed on the surface of the test location, and then concrete was poured and pounded to be compacted in layers. Three 150 mm × 150 mm × 150 mm samples shall be poured for each batch of tests. At Day 7 after concrete pouring and curing, the force transmission system shall be installed. After curing for another 1 to 2 days, the test was conducted when the uniaxial compressive strength of the concrete reached 20 MPa. Fig. 8 shows the installation of the apparatus.

In the direct shear test, the concrete specimens are firstly tested for compressive strength. When the compressive strength of the concrete samples reaches the design strength, the test can be conducted on site.

The normal stress applied to each group of specimens is determined according to an arithmetic progression. The normal stress on each test sample shall be applied in three stages, and readings taken once every 5 minutes. When the difference between two consecutive readings of vertical displacement is less than 1%, it is considered that the vertical displacement is relatively stable, and the horizontal load can be applied.

After completing each shear test, the shear friction test shall be conducted in the same way under the same normal stress. The normal stress is kept constant throughout the application of the shear stress. After the above tests, the samples should be opened and a detailed geological description of the interfaces recorded.

2.4.3 Medium-sized rock mass shear test

Specimens measuring 200 mm × 200 mm × 400 mm (length × width × thickness) were manually taken from the test location, or specimens of 200 mm in diameter and 400 mm in height were drilled. We fastened the sample with steel wire to prevent unloading and relaxation during preparation and transportation and put the lower part of the specimen into a steel mold, adjusted the shear zone plane to the horizontal, then poured the concrete, and after 3 to 4 hours, a 10-mm shear joint was reserved to pour the upper part of the concrete, so as to level the concrete surfaces. Finally, the test could be conducted after two days of curing.

A horizontal pushing method was used in the test. The normal stress acts perpendicular to the shear plane and the horizontal stress acts parallel to the shear plane. The normal stress ranged from 0 to 2.0 MPa and was applied in three stages. After the first level of normal stress was applied, pliers were used to cut the steel wire fixing the sample, and then the next two load increments were applied. The deformation was recorded at 5-minute intervals before and after loading, and a shear stress only applied after the system was relatively stable.

The shear load was applied to 10% of the estimated maximum shear load. When the shear deformation caused by loading was more than 1.5 times the previous deformation, the shear load was reduced by half until failure. The primary shear displacement and normal displacement were measured and read, allowing 5 minutes to elapse for stabilization after loading.

After the sample fails, shear friction test was performed based on the same procedure under an equivalent normal

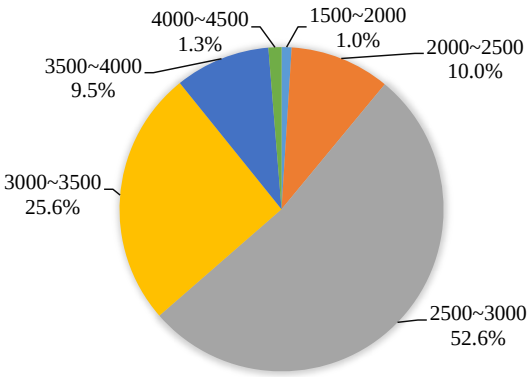

Fig. 9 Statistics of wave velocity distribution (unit: m/s)

stress. The normal stress was kept constant throughout the application of the shear stress. At the end of the test, the shear plane was described and photographed to determine the effective shear area.

3. Data and results

3.1 Loosened thickness of the natural rock mass using geophysical prospecting

The geophysical prospecting method was used to determine the thickness of loosened rock mass, which provides the basis for the depth of surface excavation at the testing location. The surface excavation of the test site is equivalent to the excavation of overburden layer of the dam foundation in reality. A total of 18 single-hole acoustic wave tests were conducted at the test site, and 686 acoustic wave signals were collected. The maximum wave velocity is 4424 m/s, the minimum wave velocity is 1845 m/s, and the average wave velocity is 2928 m/s. More detailed statistics are shown in Fig. 9, where 1.3% of the wave velocity values are between 4000 to 4500 m/s, 9.5% are between 3500 to 4000 m/s, 25.6% are between 3000 to 3500 m/s, 52.6% are between 2500 to 3000 m/s, 10.0% are between 2000-2500 m/s, and 1.0% are between 1500-2000 m/s.

A typical curve of wave velocity value versus borehole depth is given in Fig. 10. For borehole depths of 0~0.5 m, it is difficult to obtain the wave velocity data due to testing conditions, so the data corresponding to this depth range are not included; for borehole depths of 0.5~1.0 m, the wave velocities in the rock mass are small; at borehole depths greater than 1 m, the wave velocity in the rock mass gradually increases, then becomes stable.

The thickness of the loosened rock mass was determined based on the variation trend of the curve of wave velocity value *versus* hole depth. The decrease in acoustic wave velocity indicates fissure initiation and expansion at a mesoscopic level, as well as fracture generation at a macroscopic level. The effects of fissure and fracture occurrence can be characterized by the variation in the acoustic wave velocity obtained by geophysical exploration. Fig. 10 shows that the wave velocity decreases significantly in the interval up to 1 m in thickness; when the wave velocity is greater than that at a depth of 1 m, the wave

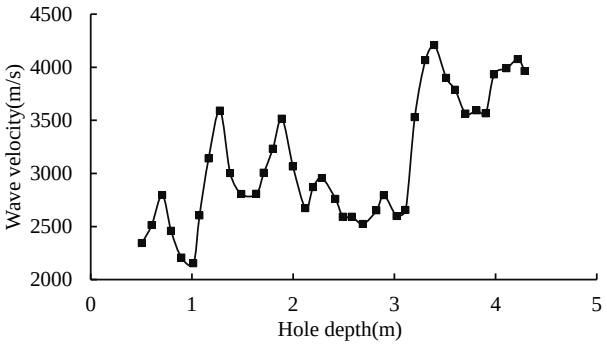

Fig. 10 Typical curve of wave velocity *versus* hole depth

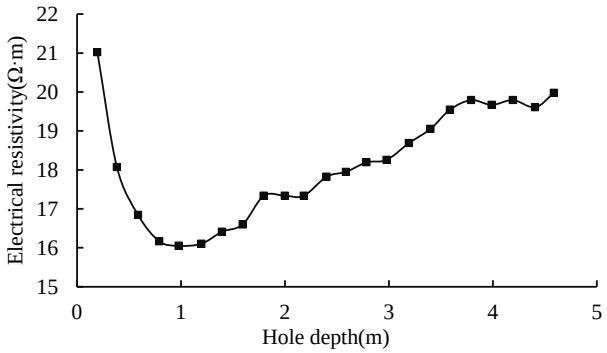

Fig. 11 Typical curve of electrical resistivity *versus* depth

velocity gradually returns to a steady state. Therefore, this method can be used to determine the depth of loosened rock at the surface of the rock mass. Combining the acoustic wave velocity and electrical resistivity data, the thickness of loosened rock mass in its natural state at the testing location can be approximately estimated as 1.0 m. It should be noted that, the geophysical prospecting method is only adopted to determine the thickness of loosened surface rock mass. Determination of mechanical parameters of rock mass, such as deformation moduli and shear strength parameters, are dependent on rock mass deformation test data, direct shear test data, *etc*.

3.2 Results of in-situ rock mass deformation tests

Fig. 12 shows the deformation curves obtained from the rock mass deformation testing considering different surface effects and plots typical field images. The deformation curves take on similar shape during the loading and unloading process. This indicates that the prepared field rock mass sites can yield rational results.

The field images considering different surface effects can also reflect the influences of various environment conditions. The rock mass surface shortly after loosened layer excavation is smooth, intact, with few fractures visible thereon (Fig. 12(b)). The rock mass surface subjected to three months' natural weathering effect is dry and coarse and a few fractures are present thereon (Fig. 12(d)). The rock mass surface subjected to dry-wet cycling for three months is overall slightly fractured and coarse and becomes a little greyer in appearance compared to neighboring rock masses (Fig. 12(f)). The rock mass surface covered by

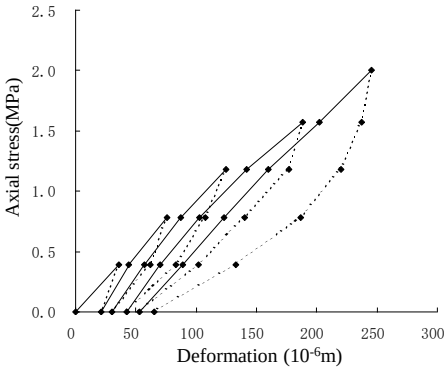

(a) deformation curve: no surface effect

(b) field image: no surface effect

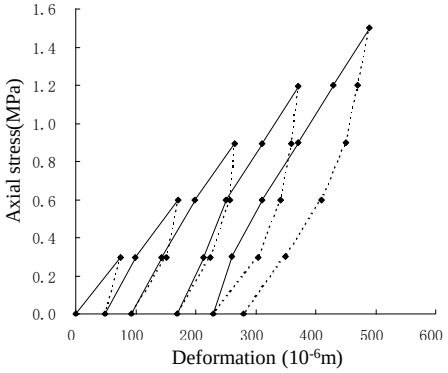

(c) deformation curve: natural weathering effect

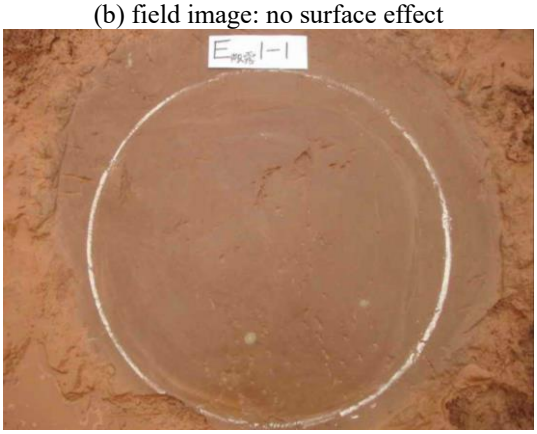

(d) field image: natural weathering effect

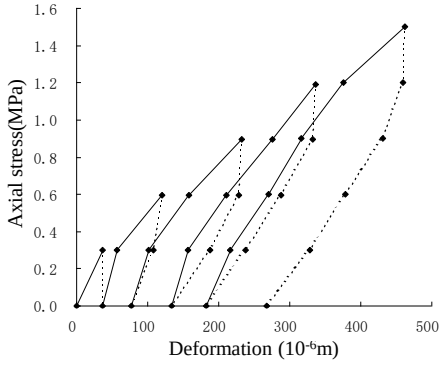

(e) deformation curve: dry-wet cycling effect

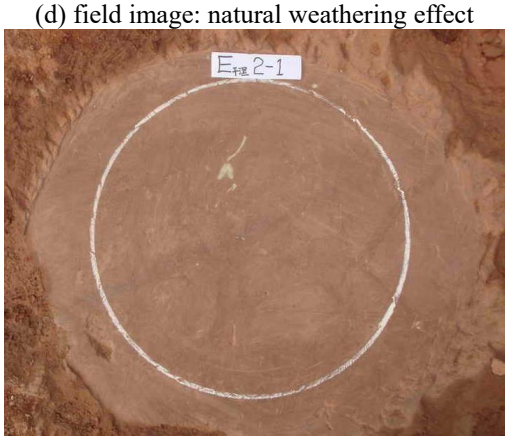

(f) field image: dry-wet cycling effect

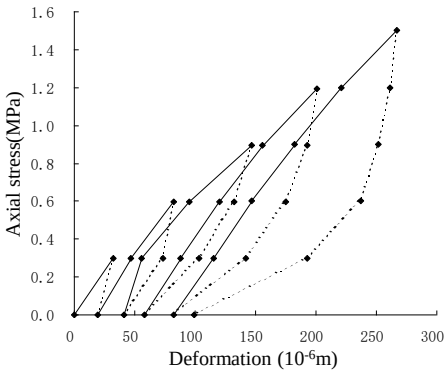

(g) deformation curve: concrete covering effect

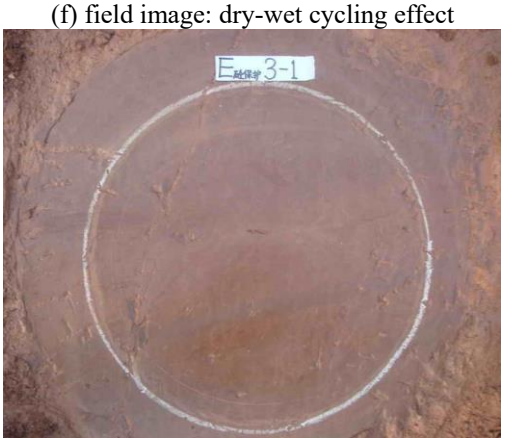

(h) field image: concrete covering effect

Fig. 12 Deformation curves and field images under various environmental conditions

Table 1 Statistics pertaining to *in-situ* rock mass deformation test results

Surface effect	No. of samples	Deformation modulus (GPa)	Average modulus (GPa)	Modulus reduction	Standard deviation (GPa)
No surface effect	E1-1	2.95	2.81	-	0.31
	E1-2	3.11			
	E1-3	2.38			
Natural weathering effect	E2-1	1.10	1.95	↓ 30.6%	0.70
	E2-2	2.82			
	E2-3	1.93			
Dry-wet cycling effect	E3-1	1.17	1.31	↓ 53.4%	0.17
	E3-2	1.22			
	E3-3	1.55			
Concrete covering effect	E4-1	2.03	2.01	↓ 28.4%	0.09
	E4-2	1.89			
	E4-3	2.10			

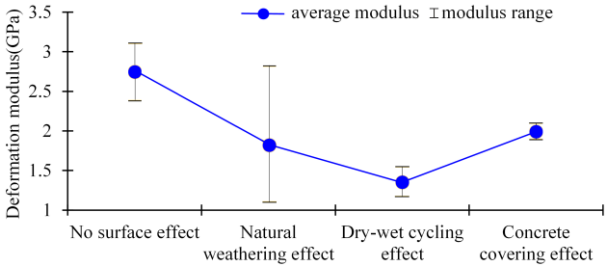

Fig. 13 Comparison of red-bed soft rock mass deformation modulus

concrete maintains its original condition (Fig. 12(h)). Different environmental effects will cause different changes in the apparent behavior and rock mass structure of the red-bed soft rock dam foundation, which may lead to changes in rock mass properties and mechanical parameters, thus affecting the bearing capacity of the dam foundation.

The statistics in Table 1 can quantitatively confirm this finding: the average rock mass deformation modulus without surface effect is 2.81 GPa, while the average magnitudes of deformation modulus corresponding to natural weathering, dry-wet cycling, and concrete cover are 1.95 GPa, 1.31 GPa, and 2.01 GPa. Fig. 13 shows that the samples subject to natural weathering vary more, which may signify that the effect caused by natural conditions is more random than other effects. A possible reason for the greater randomness lies in the fact that natural weathering is mainly manifest by sunlight, rain and ventilation conditions, and that different rock samples are affected by these factors to varying degrees, thus leading to dispersion in measured mechanical properties.

Although the data obtained from the three rock mass deformation tests conducted under each environmental condition have certain discreteness, the overall trend in the test data obtained under different environmental conditions is quite obvious after comparison. Specifically, the deformation modulus of the rock mass obtained from the deformation test conducted in a short time after the excavation of the loosened surface rock mass is the highest; the modulus obtained from the deformation test conducted after being covered with concrete for three months is a little lower; the modulus considering natural weathering effect lasting for three months is further reduced; and the minimum modulus is obtained considering the dry-wet cycling effect lasting for three months.

3.3 Results of in-situ direct shear testing of the rock-concrete interface

Fig. 14 summarizes the field direct shear test results of the interface between concrete and the rock mass under different environmental conditions, the surface of the rock mass before the direct shear test, and the interface on the rock-mass side and the interface on the concrete side after the direct shear test. Six normal stress levels are considered in each group of direct shear tests, which are distributed between 0 and 1.3 MPa. The shear strength was obtained by pushing the samples to produce shear failure, and then the Mohr-Coulomb criterion was used to obtain the cohesion and friction coefficient of the concrete-rock interface. The direct shear test images in Fig. 14 are all samples subject to zero normal stress. Observing the surface of rock mass and the interface of rock mass side and concrete side after the completion of direct shear test, the influences of different environmental conditions on the direct shear test results of rock-concrete interface can be found.

When directly pouring concrete and conducting interface direct shear testing immediately after the excavation of the loosened rock mass, the surface of the rock mass is fresh before the direct shear test (Fig. 14(b)). After the completion of the direct shear test, the exposed concrete-rock interface is generally flat, and there is a small amount of rock and concrete residue on both sides of the interface (Figs. 14(c) and 14(d)). For the tests considering natural weathering and three months' cyclic wetting-drying, the rock mass surface is already fractured before the direct shear test (Figs. 14(f) and 14(j)), and macroscopic cracks can be observed. After the direct shear tests, a certain degree of rock fracturing can be clearly observed on the side of the rock mass (Figs. 14(g) and 14(k))), while more debris is attached to the side of the concrete (Figs. 14(h) and 14(l)). For the test considering concrete cover, the rock

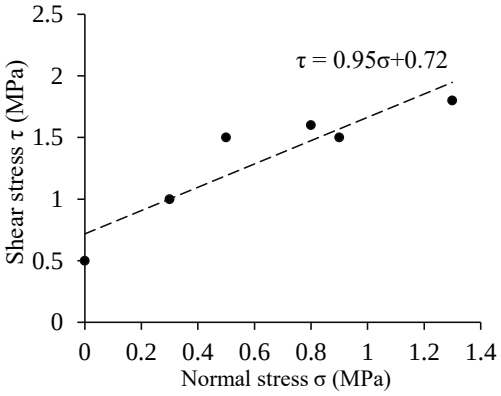

(a) curve of shear stress *v*. normal stress: no surface effect

(b) rock mass surface before pouring concrete: no surface effect

(c) rock mass after shear test: no surface effect

(d) concrete side after shear test: no surface effect

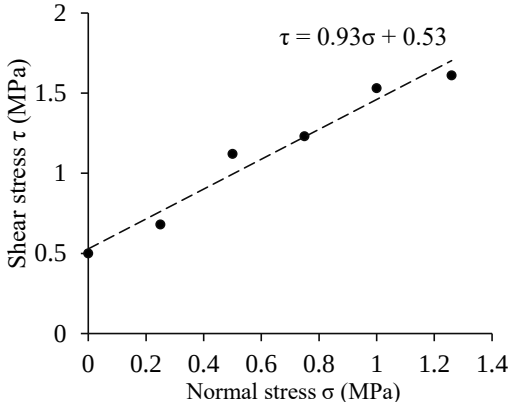

(e) curve of shear stress *v*. normal stress: natural weathering effect

(f) rock mass surface before pouring concrete: natural weathering effect

(g) rock mass side after shear test: natural weathering effect

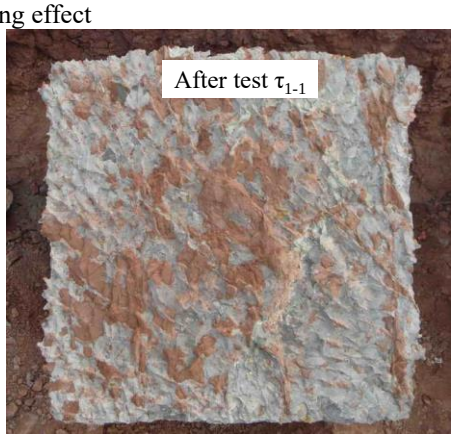

(h) concrete side after shear test: natural weathering effect

Fig. 14 Curves of shear stress *v*. normal stress and field images under various environmental conditions for the rock-concrete interface

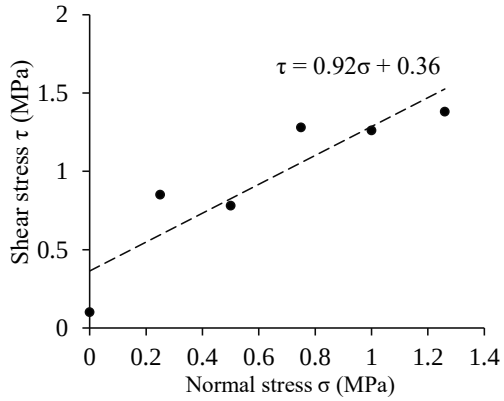

(i) curve of shear stress *v*. normal stress: dry-wet cycling effect

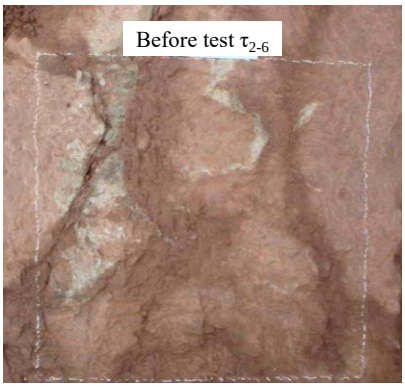

(j) rock mass surface before pouring concrete: dry-wet cycling effect

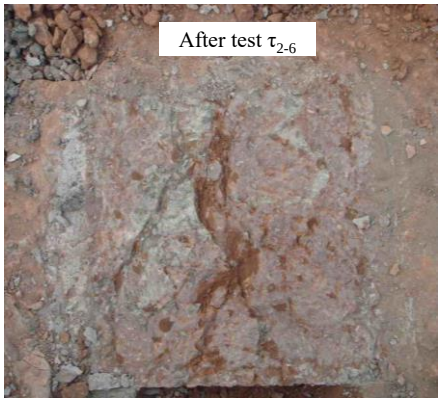

(k) rock mass side after shear test: dry-wet cycling effect

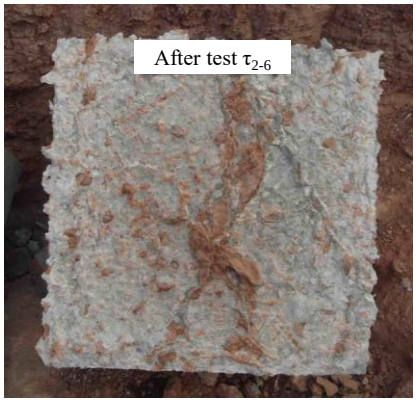

(l) concrete side after shear test: dry-wet cycling effect

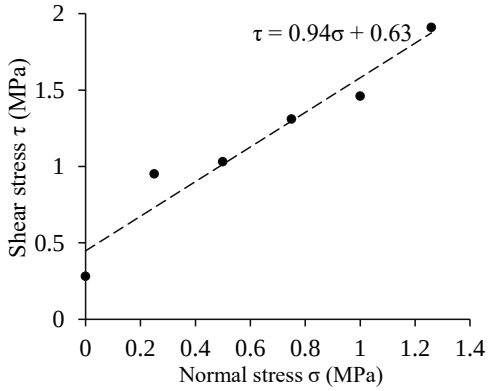

(m) curve of shear stress *v*. normal stress: concrete covering effect

(n) rock mass surface before pouring concrete: concrete covering effect

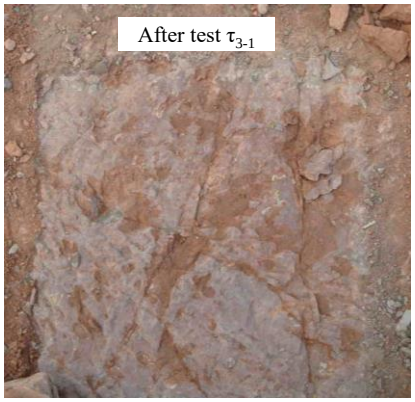

(o) rock mass side after shear test: concrete covering effect

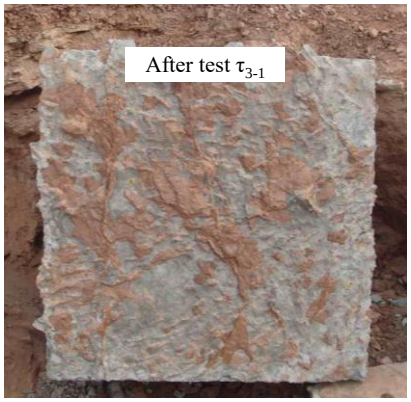

(p) concrete side after shear test: concrete covering effect

Fig. 14 Continued-

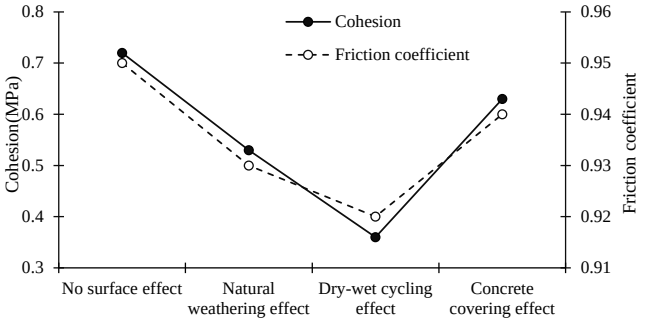

Fig. 15 Comparison of shear strength parameters of the rock-concrete interface.

Table 2 Statistical analysis of *in-situ* direct shear test data

Surface effect	Friction coefficient	Reduction	Cohesion (MPa)	Reduction
No surface effect	0.95	-	0.72	-
Natural weathering effect	0.93	↓1.1%	0.53	↓26.4%
Dry-wet cycling effect	0.92	↓2.1%	0.36	↓12.5%
Concrete covering effect	0.94	↓3.2%	0.63	↓50%

mass surface is fresh before the direct shear test, and afterwards the interface is still flat (Fig. 14(n)).

Table 2 lists statistics pertaining to data from *in-situ* direct shear tests of the rock-concrete interface. Fig. 15 further quantitatively confirms the influences of different environmental effects on the mechanical properties of the concrete-rock interface from the comparison of shear strength parameters. As can be seen, when directly pouring concrete and conducting a direct shear test immediately after the excavation of the loosened rock mass, the concrete-rock interface has the highest cohesion and friction coefficient, at 0.72 MPa and 0. 95, respectively.

The values of cohesion and friction coefficient obtained from the direct shear test are slightly reduced to 0.63 MPa and 0.94, respectively, for the concrete-rock interface which has been covered by concrete for three months before pouring additional concrete. The mechanical parameters of concrete-rock interface decrease significantly after three months of natural weathering or cyclic drying-wetting. Under natural weathering effect, the cohesion and friction coefficient of concrete-rock interface are 0.53 MPa and 0.93, respectively. Under dry-wet cycling, the cohesion and friction coefficient of concrete-rock interface are 0.36 MPa and 0.92, respectively. It can be seen from the variation that different environmental effects have more significant effects on the cohesion, and the magnitude is decreased by 12.5%, 26.4%, and 50% under the effects of concrete covering, natural weathering, and dry-wet cycling, respectively. The friction coefficient is reduced by 1.1%, 2.1%, and 3.2%, respectively. This indicates that the cohesion of the concrete-rock interface is more sensitive to different environmental effects.

Table 3 Statistics from laboratory shear tests on medium-sized rock mass specimens

Surface effect	Friction coefficient	Cohesion (MPa)	Rock mass strength (MPa)	Strength reduction
No surface effect	1.03	1.01	0.82	-
Natural weathering	0.79	0.72	0.70	↓ 14.6%
Dry-wet cycling	0.56	0.41	0.48	↓ 41.5%
Concrete covering	0.99	0.95	0.79	↓ 3.7%

3.4 Results of laboratory medium-sized rock sample shear test

Fig. 16 illustrates the results of direct shear tests of each medium-sized rock mass under different environmental conditions and the shear failure surfaces obtained from direct shear tests of the rock mass under low, intermediate, and high normal loads. The Mohr-Coulomb model was used to fit the shear strength, and the mechanical parameters of cohesion and friction coefficient of rock mass were obtained. Meanwhile, the estimated compressive strength of the rock mass was determined by using Eq. (6). The aforementioned mechanical parameters are displayed in Table 3.

$$R_{cm} = \frac{2c\cos\varphi}{1-\sin\varphi} \tag{6}$$

where $R_{0\ \mathrm{mm}}$ is compressive strength of the rock mass, c is the cohesion, and φ is the internal friction angle.

From the shear stress-normal stress data and fitting results, it can be seen (Figs. 16(a), 16(d), 16(g), 16(j)) that, the greater the normal load applied, the greater the tangential load at shear failure of the medium-sized rock mass. The normal stress and shear stress of rock mass in shear failure generally present a positive linear relationship, and the Mohr-Coulomb model used can achieve favorable fitting effect, so, the shear strength parameters obtained based on the model can reflect the shear strength characteristics of a medium-sized rock mass.

Under different normal loads, the pattern of shear failure surface of medium-sized rock mass is different. Taking the direct shear test of rock mass considering natural weathering as an example (Figs. 16(e) and 16(f)), under the low normal stress of 0.4 MPa, the shear surface of rock mass where shear failure occurs is generally flat, and the shear failure of rock mass is concentrated within a limited range above and below the failure surface. Under the highest normal stress of 2.1 MPa, the shear failure surface fluctuates, and the surface roughness is increased. The shear failure surface is very irregular with obvious serrated characteristics. With the increase of normal load, a larger range of rock mass above and below the shear failure surface is mobilized to resist the tangential force applied in the direct shear test, and then the shear capacity of the rock mass is enhanced.

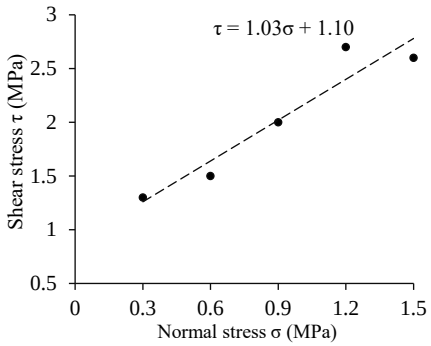

(a) curve of shear stress *v*. normal stress: no surface effect

(b) failure plane of rock mass under 0.3 MPa normal stress: no surface effect

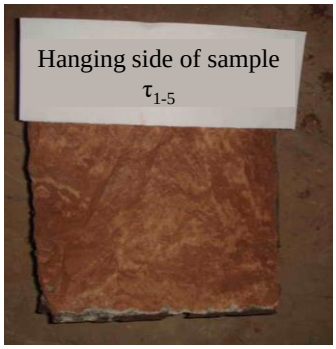

(c) failure plane of rock mass under 1.5 MPa normal stress: no surface effect

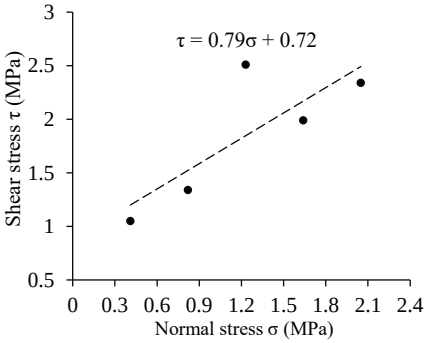

(d) curve of shear stress *v*. normal stress: natural weathering effect

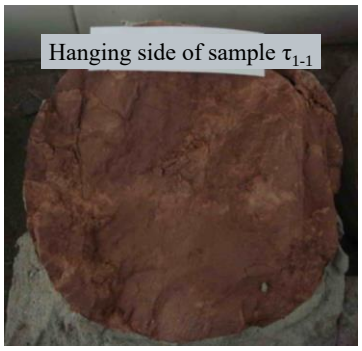

(e) failure plane of rock mass under 0.4 MPa normal stress: natural weathering effect

(f) failure plane of rock mass under 2.1 MPa normal stress: natural weathering effect

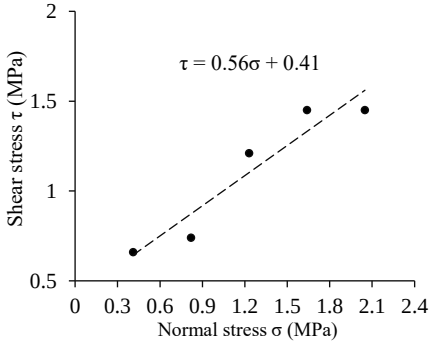

(g) curve of shear stress *v*. normal stress: dry-wet cycling effect

(h) failure plane of rock mass under 0.4 MPa normal stress: dry-wet cycling effect

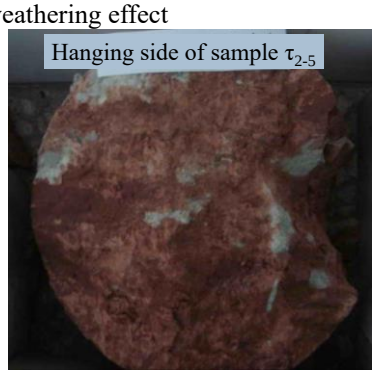

(i) failure plane of rock mass under 2.1 MPa normal stress: dry-wet cycling effect

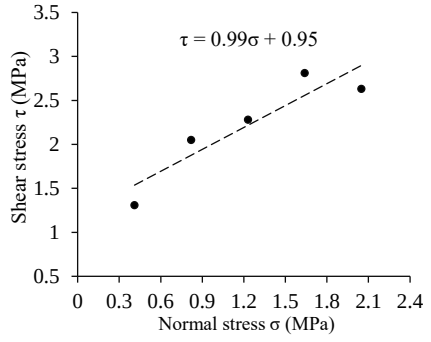

(j) curve of shear stress *v*. normal stress: concrete covering effect

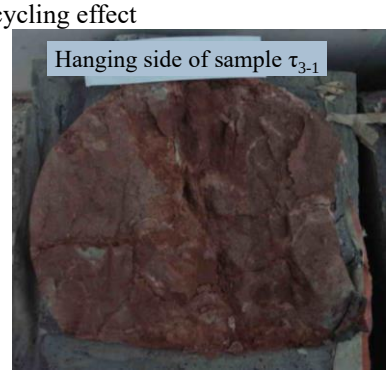

(k) concrete covering effect

(l) failure plane of rock mass under 2.1 MPa normal stress: concrete covering effect

Fig. 16 Curves of shear stress *v*. normal stress and field images under various environmental conditions for a medium-sized rock mass

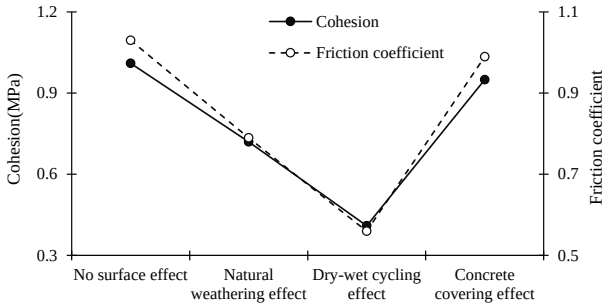

Fig. 17 Comparison of shear strength parameters of a medium-sized rock mass

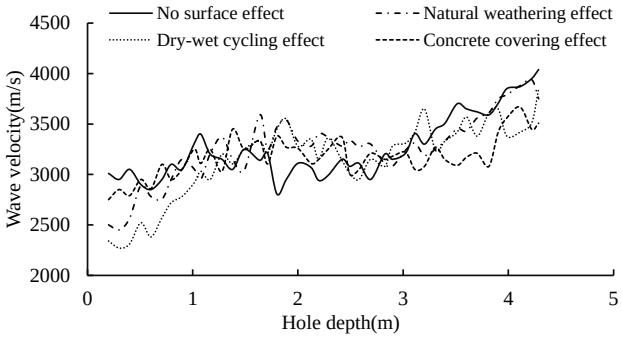

Fig. 18 Verification of test results using geophysical prospecting

Under different environmental effects, the shear strength and compressive strength of medium-sized rock mass are different. As shown in Fig. 17, the cohesion and friction coefficient without considering any environmental effect are 1.01 MPa and 1.03 respectively. The cohesion and friction coefficient are 0.72 MPa and 0.79, 0.41 MPa and 0.56, and 0.95 MPa and 0.99, respectively, under natural weathering, dry-wet cycling, and concrete cover, respectively. The compressive strength of a rock mass is a comprehensive index used to characterize the bearing capacity and mechanical properties thereof. By analyzing this index, the compressive strength of rock mass without considering environmental influences is found to be 0.82 MPa. The compressive strengths considering natural weathering, dry-wet cycling, and concrete cover are 0.70 MPa, 0.48 MPa, and 0.79 MPa with corresponding decreases of 14.6%, 41.5%, and 3.7%, respectively.

3.5 Verification of the mechanical test results

To verify the mechanical test results, geophysical prospecting was used again to investigate the loosened thickness of the rock mass under different environmental effects. For each testing area (Fig. 4), a test-hole was drilled and the acoustic wave velocity variation with hole depth measured. Fig. 18 shows changes in wave velocity with hole depth. The curve denoted as "no surface effect" refers to the results derived from the test shortly after the excavation, while the other three curves refer to the results derived from tests after three months subject to different environmental effects.

The wave velocity *versus* hole depth curves can verify the mechanical test findings. Fig. 18 reveals that the wave velocity magnitudes corresponding to "no surface effect" and "concrete covering effect" are close and the loosened extent of rock mass is not obvious. This conclusion is consistent with the mechanical test data, in which the mechanical parameters under these two scenarios are similar. Furthermore, the wave velocity curves corresponding to "natural weathering" and "dry-wet cycling" exhibit significant decreases within depths of 0.4 m and 0.8 m, respectively, indicating a more significant effect on the mechanical performance of the rock mass.

This conclusion also agrees with the variations obtained by the aforementioned mechanical tests, therefore, the mechanical test results can be verified using the wave velocity index in a qualitative manner.

4. Analysis and discussions

4.1 Analysis of geophysical prospecting and in-situ testing results

The mechanical test results conducted *in-situ* show that the rock mass used for the test is in an undisturbed state, so the test results have good regularity and can reflect the influences of different environmental effects. This shows that it is necessary to excavate the loosened rock mass on the surface for the red-bed soft rock. The geophysical exploration technique used in the present investigation can realize an accurate detection of the thickness of the surface loosened rock mass, and therefore provide an effective guidance for *in-situ* mechanical testing. Therefore, it is suggested that the geophysical prospecting method should be further extended to the detection of the loosened thickness of the surface rock mass at the dam foundation site in the subsequent actual construction of the red-bed soft rock dam foundation. Thus, the reasonable treatment thickness of the surface loosened rock mass of the dam foundation can be recommended.

In this study, three kinds of environmental effects including natural weathering, dry-wet cycling, and concrete covering were designed. The deformation modulus of the rock mass, the shear strength of concrete-rock interface, the shear strength and compressive strength of rock mass under each environmental effect were obtained by *in-situ* mechanical tests on the rock. These indices comprehensively represent the mechanical properties and bearing capacity condition of the red-bed soft rock dam foundation rock mass and are important parameters for dam design and construction. By comparing the variation of these parameters, it is found that under concrete cover, the mechanical properties of red-bed soft rock decrease, but the decrease is generally limited, and the bearing capacity of rock mass can be maintained. This indicates that, under the sealing effect of concrete, the rock mass structure characteristics remain unchanged, and there are few new cracks initiated and expanding in the rock mass, so there is no significant influence on the macro-mechanical parameters of the rock mass. Under natural weathering, the mechanical parameters of red-bed soft rock decrease to a certain extent, which indicates that after the excavation of the dam foundation rock mass, if it is left unsealed for a long time, the surface rock mass will be affected by

weathering and unloading, and weathering fissures and unloading fissures will be formed in the surface layer and gradually expand to the shallow layer, resulting in deterioration of its mechanical properties and reduced macro-mechanical parameters. The mechanical parameters of red bed soft rock decrease to the greatest extent under the effect of dry-wet cycling. This is because the effect of dry-wet cycling is not only contributed to by weathering, but also influenced by water-rock interaction. Through the fissures produced by weathering, water will infiltrate the red-bed soft rock, resulting in the reaction between water and hydrophilic minerals in the rock mass, weakening the rock mass.

Furthermore, dam foundations are generally built on riverbeds, where a certain thickness of loosened overburden is present due to the geological action and scouring of the water over time. Therefore, the geological condition of the riverbed should be identified by drilling boreholes before construction of the dam. The method proposed herein is equally applicable to the detection of the loosened depth of a riverbed under actual engineering conditions. Depending on the actual conditions, the length of a geophysical prospecting hole can cover the depth of the loosened overburden and reach fresh bedrock beneath, therefore, the proposed methods and procedures regarding geophysical prospecting and mechanical tests are applicable to actual engineering conditions.

4.2 Implications for dam construction

The variations in the mechanical properties of a red-bed soft rock dam foundation under different environmental conditions provide some useful implications for the scheduled dam construction on red-bed soft rock.

(1) The *in-situ* rock mass mechanical test data show that the rock-mass mechanical properties are best in the absence of environmental effects. This indicates that the rock mass of the dam foundation should be timely treated, such as grouting reinforcement or dam concrete pouring, thus maximizing the bearing capacity of the rock mass.

(2) Natural weathering over three months is considered in the *in-situ* mechanical testing. This corresponds to the possible situation that the rock mass is exposed without treatment after the surface loosened rock mass is cleared and excavated. The test results show that, in this situation, the mechanical properties and bearing capacity of rock mass will be reduced, which is not beneficial to subsequent dam construction. Therefore, it is suggested that the rock mass forming the dam foundation should not be left exposed overly long after excavation in the actual construction to prevent the adverse effects of weathering and unloading. If unexpected factors are encountered in the actual project and timeous treatment cannot be carried out, as a measure to slow down the weathering and unloading process, it is suggested that the measures such as tarpaulin should be used to cover the dam foundation.

(3) Dry-wet cycling over three months is considered in the in-situ rock mass mechanical testing. In engineering practice, if the rock mass forming the dam foundation is not treated for a long time and experiences alternation under rainfall and sunshine, the adverse effects are akin to those considered in the mechanical testing. The test results and analysis show that the effect of this environmental regime on the dam foundation rock mass is the most significant, and water is an important factor driving the deterioration of the rock mass. Therefore, it is suggested that the influence of water on the excavated dam foundation should be strictly controlled in practice. For example, to keep the rock mass of the dam foundation in a natural state, construction water should be restricted so as not to converge on the dam foundation surface, and waterproof tarpaulin should be laid timeously to avoid the impact of rainwater. At the same time, screening to prevent direct incidence of sunlight on the rock should be implemented to prevent the water content of the rock mass from decreasing.

(4) The concrete covering effect lasting for three months is considered in the *in-situ* mechanical tests. In practice, this situation corresponds to the dam foundation rock mass being re-exposed after removing the existing hydraulic structures on the dam foundation. According to the *in-situ* mechanical test results, the bearing capacity of the studied dam foundation rock mass decreases slightly, but the overall mechanical properties do not change significantly. Therefore, during the demolition and reconstruction of hydraulic structures on the red-bed soft rock dam foundation, the bearing capacity of the re-excavated dam foundation rock mass can be considered to be unchanged, and the mechanical properties of the dam foundation rock mass continue to be represented by the previously used parameters.

5. Conclusions

Extensive investigations were conducted on the red-bed soft rock, including geophysical prospecting and a series of *in-situ* mechanical tests. The rock mass of the red-bed soft rock dam foundation was tested under different environmental conditions; the key conclusions are as follows:

(1) The geophysical prospecting method can reveal that the weathering unloading depth of the surface rock mass of red-bed soft rock is about 1 m, which provides an accurate basis for the excavation of the surface loosened rock mass;

(2) Different environmental effects have different effects on the mechanical properties of such rock masses. Specifically, under the effect of concrete sealing, the mechanical properties of the rock mass remain unchanged. Under the effect of natural weathering, the mechanical parameters of the rock mass decrease to a certain extent; under the effect of dry-wet cycling, the mechanical parameters decrease significantly. The compressive strengths of rock mass are 0.79 MPa, 0.70 MPa, and 0.48MPa under the effects of concrete sealing, natural weathering, and dry-wet cycling, respectively (some 3.7%, 14.6%, and 41.5% lower than the compressive strength of the freshly excavated dam foundation rock mass of 0.82 MPa). The analysis shows that weathering and unloading after excavation will cause the initiation and expansion of cracks in the rock mass, thus affecting its macro-scale mechanical parameters. In

addition, water-rock interaction will weaken the rock mass, leading to a reduced bearing capacity;
(3) Through mechanical testing and analysis of different environmental effects, useful implications arise for the construction of a dam foundation on such red-bed soft rock, including timeous application of grouting reinforcement or concrete pouring after the excavation of the loosened rock mass, and reliable waterproofing measures, and measures for preventing weathering and unloading (these also involve shading to protect the exposed rock mass to direct sunlight and limit evaporation of the moisture therein).

Acknowledgments

The work was supported by the Fundamental Research Funds for the Central Institutes of China (Nos. CKSF2023316/YT, CKSF2023307/YT, CKSF2021463/YT). These supports are greatly acknowledged.

References

Aehnelt, M., Hilse, U., Pudlo, D., Heide, K. and Gaupp, R. (2021), "On the origin of bleaching phenomena in red bed sediments of Triassic Buntsandstein deposits in Central Germany", *Geochemistry*, **81**(2), 125736. https://doi.org/10.1016/j.chemer.2020.125736.

Azarafza, M., Ghazifard, A., Akgun, H. andAsghari-Kaljahi, E. (2019), "Geotechnical characteristics and empirical geo-engineering relations of the South Pars Zone marls, Iran", *Geomech. Eng.*, **19**(5), 393-405. https://doi.org/10.12989/gae.2019.19.5.393.

Chen, S.H., Yang, Z.M., Wang, W.M. and Shahrour, I. (2012), "Study on rock bolt reinforcement for a gravity dam foundation", *Rock Mech. Rock Eng.*, **45**(1), 75-87. https://doi.org/10.1007/s00603-011-0179-9.

Chen, G., Yang, J.S., Liu, Y., Kitahara, T. and Beer, M. (2023), "An energy-frequency parameter for earthquake ground motion intensity measure", *Earthq. Eng. Struct. D.*, **52**(2), 271-284. https://doi.org/10.1002/eqe.3752.

He, J.L., Niu, F.J., Luo, F., Jiang, H.Q., He, P.F. and Ju, X. (2023), "Mechanical properties and modified binary–medium constitutive model for red–bed soft rock subjected to freeze–thaw cycles", *Cold Reg. Sci. Technol.*, **209**, 103803. https://doi.org/10.1016/j.coldregions.2023.103803.

Huang, W., Jackson, M.J., Dekkers, M.J., Solheid, P., Zhang, Y., Li, S. andDing, L. (2020), "Remagnetization of red beds on the Tibetan Plateau: Mechanism and diagnosis", *J. Geophys. Res. Solid Earth*, **125**(8), e2020JB020068, https://doi.org/10.1029/2020JB020068.

Koshnaw, R.I., Stockli, D.F. and Schlunegger, F. (2019), "Timing of the Arabia-Eurasia continental collision—Evidence from detrital zircon U-Pb geochronology of the Red Bed Series strata of the northwest Zagros hinterland, Kurdistan region of Iraq", *Geology*, **47**(1), 47-50. https://doi.org/10.1130/G45499.1.

Jiang, H. and Qiu, X. (2021), "Performance assessment of a newly developed and highly stable grouting material for a completely weathered granite dam foundation", *Constr. Build. Mater.*, **299**, 123956. https://doi.org/10.1016/j.conbuildmat. 2021.123956.

Jiang, Q., Wang, B., Feng, X.T., Fan, Q.X., Wang, Z., Pei, S. and Jiang, S. (2019), "In situ failure investigation and time-dependent damage test for columnar jointed basalt at the Baihetan left dam foundation", *Bull. Eng. Geol. Environ.*, **78**(6), 3875-3890. https://doi.org/10.1007/s10064-018-1399-y.

Li, A.R., Deng, H., Zhang, H.J., Liu, H.H. and Jiang, M.L. (2023), "The shear-creep behavior of the weak interlayer mudstone in a red-bed soft rock in acidic environments and its modeling with an improved Burgers model", *Mech. Time-Dependent Mater.*, **27**, 1-18. https://doi.org/10.1007/s11043-021-09523-y.

Liu, Z., He, X.F., Fan, J. and Zhou, C.Y. (2019), "Study on the softening mechanism and control of red-bed soft rock under seawater conditions", *J. Mar. Sci. Eng.*, **7**(7), 235. https://doi.org/10.3390/jmse7070235.

Liu, Z., He, X.F. and Zhou, C.Y. (2019), "Influence mechanism of different flow patterns on the softening of red-bed soft rock", *J. Mar. Sci. Eng.*, **7**(5), 155/ https://doi.org/10.3390/jmse7050155/

Marat, A.R., Tămaş, T., Samşudean, C. and Gheorghiu, R. (2022), "Physico-mechanical and mineralogical investigations of red bed slopes (Cluj-Napoca, Romania)", *Bull. Eng. Geol. Environ.*, **81**(2), 1-20. https://doi.org/10. 1007/ s10064-021-02542-6.

Shahrbanouzadeh, M., Barani, G.A. and Shojaee, S. (2015), "Analysis of flow through dam foundation by FEM and ANN models Case study: Shahid Abbaspour Dam", *Geomech. Eng.*, **9**(4), 465-481. https://doi.org/10.12989/gae.2015. 9. 4.465.

Shen, P.W., Tang, H.M., Huang, L. and Wang, D.J. (2019), "Experimental study of slaking properties of red-bed mudstones from the Three Gorges Reservoir area", *Mar. Georesour. Geotech.*, **37**(8), 891-901. https://doi.org/10.1080/1064119X.2018.1504839.

Trümper, S., Gaitzsch, B., Schneider, J.W., Ehling, B.C., Kleeberg, R. and Rößler, R. (2020), "Late Palaeozoic red beds elucidate fluvial architectures preserving large woody debris in the seasonal tropics of central Pangaea", *Sedimentology*, **67**(4). 1973-2012. https://doi.org/10.1111/sed.12692.

Varmazyari, M., Sabbagh-Yazdi, S.R. and Mirzabozorg, H. (2021), "Coupled arch dam-reservoir-massed foundation problem under different earthquake input mechanisms", *Coupled Syst. Mech.*, **10**(5), 371-392. https://doi.org/10.12989/csm.2021.10.5.371.

Wang, X., Liu, Y., Tao, Z., Wang, W. and Yang, Q. (2020), "Study on the failure process and nonlinear safety of high arch dam and foundation based on geomechanical model test", *Eng. Fail. Anal.*, **116**, 104704. https://doi.org/10.1016/j.engfailanal.2020.104704.

Wilmsen, M., Fürsich, F.T., Seyed-Emami, K. and Majidifard, M. R. (2021). "The upper Jurassic Garedu red bed formation of the northern tabas block: Elucidating late cimmerian tectonics in east-central Iran", *Int. J. Earth Sci.*, **110**(3), 767-790. https://doi.org/10.1007/s00531-021-01988-z.

Wu, B., Niu, J., Su, H., Yang, M., Wu, Z. and Cui, X. (2019), "An approach for deformation modulus mechanism of super-high arch dams", *Struct. Eng. Mech.*, **69**(5), 557-566. https://doi.org/10.12989/sem.2019.69.5.557.

Yan, L., Peng, H., Zhang, S., Zhang, R., Kašanin-Grubin, M., Lin, K. and Tu, X. (2019), "The spatial patterns of Red Beds and Danxia Landforms: Implication for the formation factors–China", *Scientific Reports*, **9**, 1961. https://doi.org/10.1038/ s41598-018-37238-7

Yilmaz, D., Altunisik, A.C. and Adanur, S. (2021), "Deformation modulus of rock foundation in Deriner Arch Dam. *Geomech. Eng.*, **26**(1), 63-75. https://doi.org/10.12989/ gae.2021.26.1.063.

Yu, L., Lai, H.Q., Zhou, C.Y., Liu, Z. and Zhang, L.H. (2022), "Percolation threshold of red-bed soft rock during damage and destruction", *Appl. Sci.*, **12**(15), 7615. https://doi.org/10.3390/app12157615.

Zhang, Z.T. and Gao, W.H. (2020), "Effect of different test methods on the disintegration behavior of soft rock and the evolution model of disintegration breakage under cyclic wetting and drying", *Eng. Geol.*, **279**, 105888. https://doi.org/10.1016/j.enggeo.2020.105888.

Zhou, C.Y., Xu, Yang., Liang, Y.H., Du, Z.C., Liu, Z., Huang, W., and Ming, W.H. (2019), "Classification of red-bed rock mass structures and slope failure modes in South China", *Geosciences*, **9**(6), 273. https://doi.org/10.3390/geosciences9060273.

Zhou, M., Li, J., Luo, Z., Sun, J., Xu, F., Jiang, Q. and Deng, H. (2021), "Impact of water–rock interaction on the pore structures of red-bed soft rock", *Scientific Reports*, **11**, 1-15. https://doi.org/10.1038/s41598-021-86815-w

CC